ACS APPLIED MATERIALS & INTERFACES

Research Article

www.acsami.org

Synthesis and Extreme Rate Capability of Si−Al−C−N Functionalized Carbon Nanotube Spray-on Coatings as Li-Ion Battery Electrode

Lamuel David, Deepu Asok, and Gurpreet Singh*

Mechanical and Nuclear Engineering Department, Kansas State University, Manhattan, Kansas 66506, United States

Supporting Information

ABSTRACT: Silicon-based precursor derived glass-ceramics or PDCs have proven to be an attractive alternative anode material for Li ion batteries. Main challenges associated with PDC anodes are their low electrical conductivity, first cycle loss, and meager C-rate performance. Here, we show that thermal conversion of single source aluminum-modified polysilazane on the surfaces of carbon nanotubes (CNTs) results in a robust Si−Al−C−N/CNT shell/core composite that offers extreme C-rate capability as battery electrode. Addition of Al to the molecular network of Si−C−N improved electrical conductivity of Si−C−N by 4 orders of magnitude, while interfacing with CNTs showed 7-fold enhancement. Further, we present a convenient spray-coating technique for PDC composite electrode preparation that eliminates polymeric binder and conductive agent there-by reducing processing steps and eradicating foreign material in the electrode. The Si−Al−C−N/CNT electrode showed stable charge capacity of 577 mAh g^{-1} at 100 mA g^{-1} and a remarkable 400 mAh g^{-1} at 10 000 mA g^{-1}, which is the highest reported value for a silazane derived glass-ceramic or nanocomposite electrode. Under symmetric cycling conditions, a high charge capacity of ∼350 mA g^{-1} at 1600 mA g^{-1} was continuously observed for over 1000 cycles.

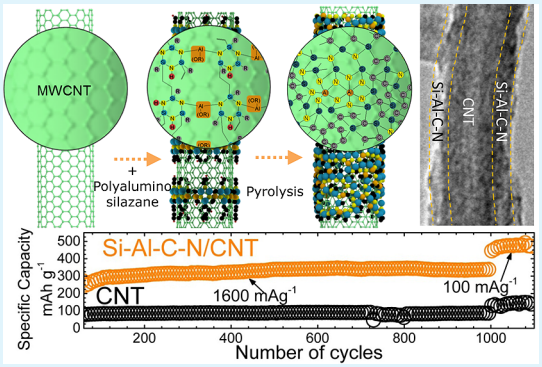

KEYWORDS: *carbon nanotubes, Li-ion battery, anode, silicon, silazane, ceramics*

INTRODUCTION

The future success of battery operated vehicles and portable electronic devices will require invention of lightweight, safer, high capacity, long lasting and high power electric sources. From a practical standpoint, advanced lithium ion battery technology (*a*-LIB) seems to be the most viable option.[1−8] Therefore, considerable improvements to the present-day LIB electrode and electrolyte materials and design are needed to achieve high rate capability, short charging time, high energy density, and long cycle life.[9−11] Accordingly, much of the research emphasis has been on the development of high capacity anode materials; particularly silicon anodes because of its high theoretical lithium discharge capacity of 3850 mAh·g^{-1} (>10 times that of commercial graphite).[10,11] Traditional silicon however has other shortcomings such as low electrical conductivity, large volumetric changes that cause cracking, and unstable solid electrolyte interphase (SEI) formation that leads to poor C-rate and capacity fading.[11−14] Consequently, several silicon nanostructured electrode design and 3-D assemblies involving shell/core nanowires, nanorods, microspheres and particles etc. have been proposed and fabricated.[15−24] These new designs have considerably alleviated many of the issues, however, the relatively low volumetric energy densities and challenges associated with their large-scale production and high manufacturing cost must be overcome before such technologies can be commercialized.

Among other anode materials for *a*-LIBs, silicon-based precursor derived glass ceramics (or PDCs) such as silicon carbonitride (or Si−C−N) have shown incredible electrochemical performance in recent years. These glass-ceramics, known for their aberrant nanodomain structure (characterized by two interpenetrating amorphous phases of Si−C−N mixed bonds and excess disordered carbon), show Li discharge capacities almost twice that of commercial graphite anode.[26−36] The presence of carbon embedded in phases of Si−C−N mixed bonds in the matrix makes these materials incredibly good in Li storage than free-standing carbon. PDCs however suffer from poor rate performance, high first cycle loss, and voltage hysteresis that is generally attributed to low electrical conductivity, and formation of Li-irreversible phases during the first discharge.[37] One way to overcome these issues is perhaps by alteration of molecular structure of the preceramic polymer with a quaternary element that can improve the conductivity and rate capability of the pyrolyzed ceramic. It is well-known that introduction of foreign elements (e.g., B, Al, Hf, etc.) into the molecular network of Si−C−N have benefits such as extraordinary resistance to crystallization and oxidation resistance (1400−1700 °C),[38−42] creep resistance[43−46] and most importantly have better electric property.[47,48] Enhanced

Received: June 20, 2014
Accepted: September 1, 2014
Published: September 1, 2014

 © 2014 American Chemical Society

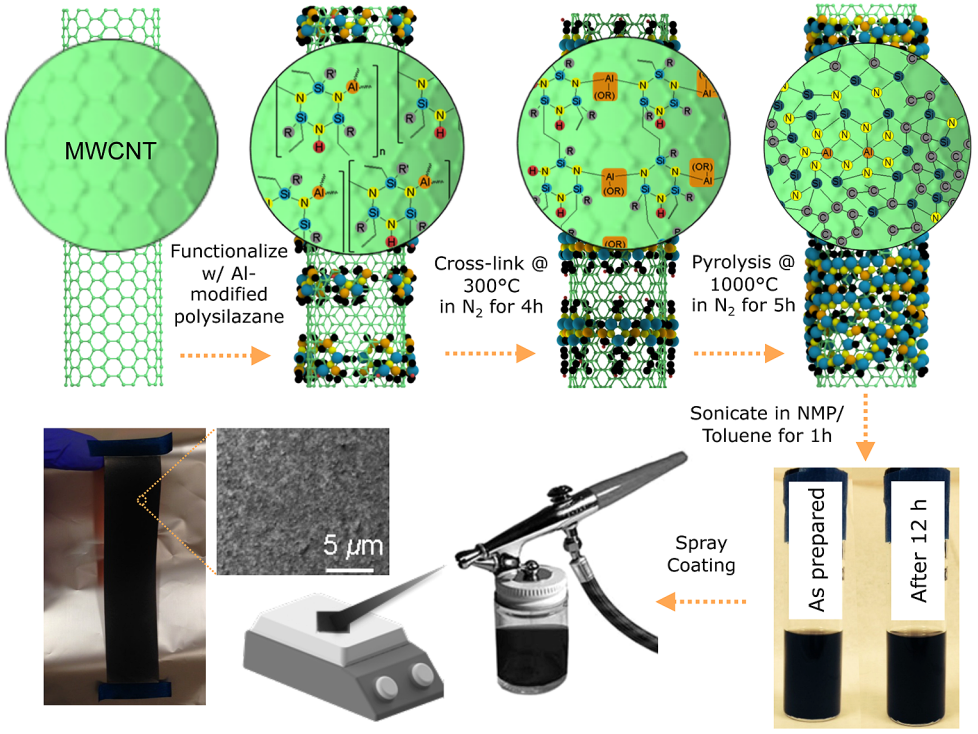

Figure 1. Schematic showing overall approach toward synthesis of Si−Al−C−N/CNTs composite and electrode preparation by spray-coating technique. (L to R): Al doped polymeric precursor wets the CNT surface forming a uniform layer. During heating in flowing N_2, the polymer first cross-links at 300 °C forming a 3-D network where Al is preferentially enriched in string-like regions separated by Al-poor regions. Later, during pyrolysis the reaction of aluminum alkoxide with Si−H and N−H bonds facilitates homogeneous distribution of aluminum in flexible chainlike blocks along with large Si−N rings throughout the matrix. The as-obtained ceramic/CNT is then sonicated in toluene/NMP mix to form stable dispersion, which is then spray coated onto a Cu foil (approximately 6 in. × 2 in.) kept on a hot plate.

electrical conductivity due to Al doping of Si−C−N would prove vital in improving electron transport in the electrode at nanolevel, there-by boosting its electrochemical performance. Further improvements in rate capability of PDC electrode could be expected by nanostructuring;[4,11,20,25] blending PDCs with carbon nanotubes (CNTs) in the form of shell/core geometry is expected to further enhance electrical conductivity, Li-ion accessibility i.e., provide smooth channels for ion-transportation, and offer an elastic support for spatial expansion/contraction during intercalation/extraction of Li ions.[49−57]

To test this hypothesis, we demonstrate the processing and electrochemical behavior of Si−Al−C−N/CNT hybrid composite that shows incredible capacity along with long cyclic stability even at unmatched current density of 10 000 $mA{\cdot}g^{-1}$. We also demonstrate an alternate approach to PDC anode preparation. In traditional cells, where the electrode is prepared by slurry coating a mixture of active material with conducting agent (generally carbon black) and polymeric binders in 8:1:1 ratio, our anode is prepared by spray coating of the as-prepared composite dispersions directly onto the metal current collector foil.

EXPERIMENTAL SECTION

Materials and Instrumentation. Aluminum propoxide (99.9%) was purchased from Sigma-Aldrich. Poly(ureamethylvinyl)silazane (Ceraset) was obtained from Clariant Corporation. All materials were used as received without further purification.

Scanning electron microscopy (SEM) of the synthesized material was carried out on Carl Zeiss EVO MA10 system with incident voltage of 5−30 kV. TEM images were digitally acquired by use of a Phillips CM100 and FEI CM200 operated at 100 kV. The FTIR spectra were collected using Thermo-Nicolet Nexus 870FT-IR spectrometer. FTIR samples were prepared by mixing ∼1 wt % of the finely powdered sample with FTIR grade KBr powder. Thermogravimetric analysis was performed using Shimadzu 50 TGA (Columbia, MD) (limited to 1000 °C). Sample weighing, ∼5 mg, was heated in a platinum pan at a rate of 10 °C/min in air flowing at 10 mL/min. XRD spectrum was obtained using Bruker powder X-ray diffractometer (Madison, WI) operating at room temperature, with CuKα radiation and nickel filter. The pyrolyzed samples were finely crushed with mortar and pestle and laid on the palette for analysis. Raman spectra were measured using a LabRAM ARMIS Raman spectrometer using 633 nm laser excitation (laser power of 17 mW) as the light source. SS-NMR Experiments were carried out on a Bruker Avance II 300 spectrometer (Billerica, MA) operating at a static magnetic field of 7.05 T. The surface chemical composition was studied by X-ray photoelectron spectroscopy (XPS, PHI Quantera SXM) using monochromatic Al Kα X-ray radiation.

Preparation of Si−Al−C−N/CNT. The "as-obtained" 1 g of CNTs (Arkema) were dispersed in 1 g L^{-1} sodium dodecyl benzenesulfonate (NaDDBS) (Sigma-Aldrich) aqueous solution, followed by sonication for 1h to remove any unwanted agglomerations. The dispersed nanotubes were then washed repeatedly with DI water to eliminate any excess NaDDBS or related impurities, followed by slow drying that yielded a dry CNT mass. These dried nanotubes (approximately 1 g) were then dispersed in toluene (125 mL) for further functionalization. The Al-modified polymeric precursor was prepared by following a procedure somewhat similar to that described by Dhamne et al.;[39] aluminum propoxide was added to polysilazane in 10:90 weight ratio followed by physical mixing at room temperature. The precursor was then slowly added and stirred in the 5 wt % CNT dispersed in toluene. After the mix was stirred for approximately 24 h, it was dried in inert atmosphere at 80 °C. The dried mix was then transferred to a tube furnace where it was heated to 300 °C for

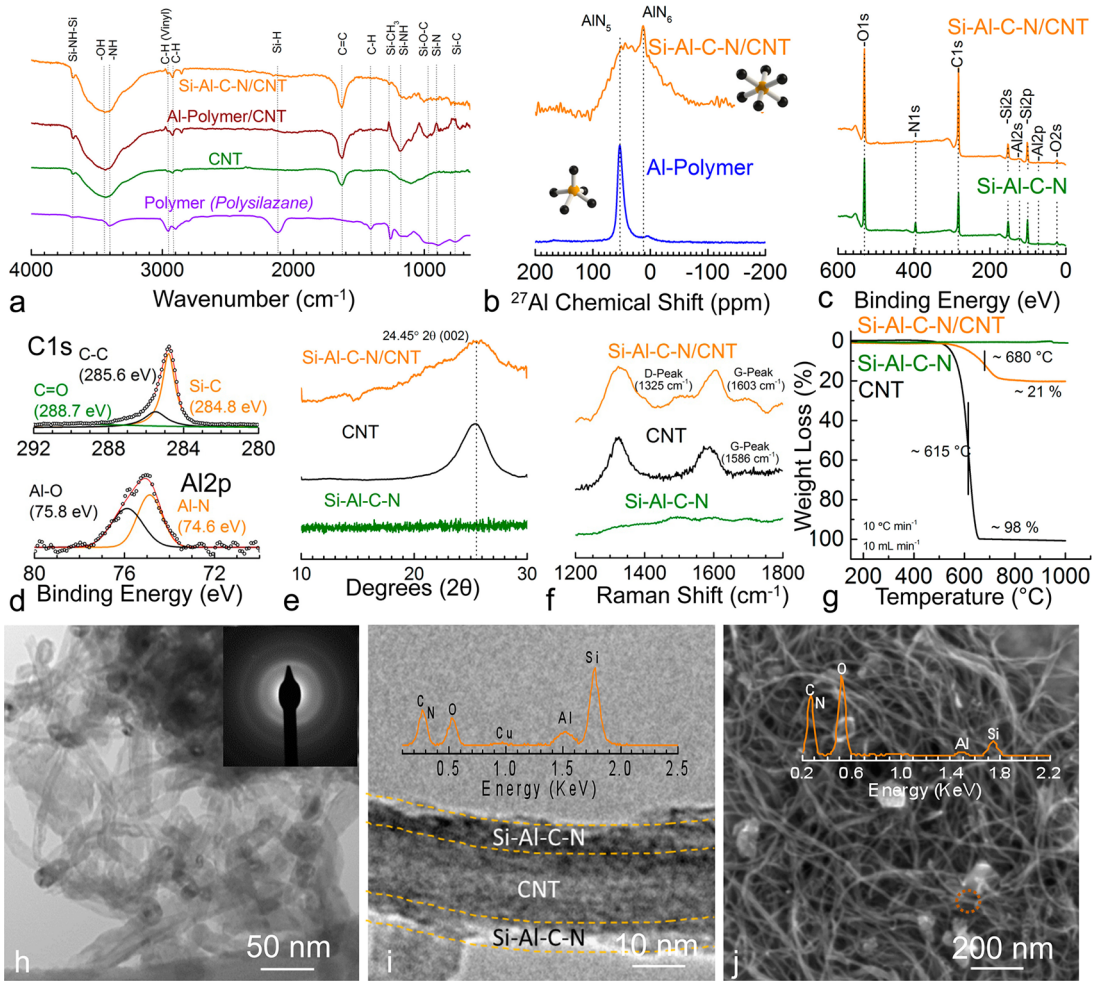

Figure 2. Material characterization. (a) FTIR comparison of Si−Al−C−N/CNT (before and after pyrolysis) and CNTs along with the as-obtained polysilazane precursor. (b) ^{27}Al NMR spectra of Si−Al−C−N/CNT and Al modified polysilazane polymer. (c) X-ray photoelectron spectroscopy plot of Si−Al−C−N and Si−Al−C−N/CNTs. Peak characteristic to Al 2s and Al 2p could be observed in both the specimens. (d) High-resolution XPS of Si−Al−C−N/CNTs composite showing the characteristic C 1s and Al 2p peaks. (e) XRD data confirming the amorphous structure of Si−Al−C−N and presence of CNTs in Si−Al−C−N/CNTs. (f) Comparison of Raman spectra of CNTs and Si−Al−C−N/CNTs. The characteristic D- and G-peaks are clearly observed. (g) Thermogravimetric analysis plot of CNTs and Si−Al−C−N/CNTs hybrid composite. (h) low and (i) high resolution TEM images of Si−Al−C−N/CNT. Inset: SAED pattern and EDX spectra obtained from the corresponding TEM images. (j) SEM images showing the spray coated Si−Al−C−N/CNT electrode on Cu current collector foil. The EDX spectra of the spots shown in the corresponding SEM image indicating the material to be Si−Al−C−N.

approximately 4 h for cross-linking of the precursor, followed by a pyrolysis at 1000 °C for 5 h in nitrogen atmosphere at 5 °C min^{-1} heating and cooling rates to yield Si−Al−C−N/CNT composite. These heating and cooling rates are typical for PDC composites.[41,53]

The Si−Al−C−N powder specimen was prepared in a similar manner as described above. Briefly, liquid Al-modified polymeric precursor was cross-linked in a vertical tube furnace at approximately 300 °C in N_2 for 4 h resulting in an infusible mass, which was ball milled for 2 h and pyrolyzed at 1000 °C for 5 h in N_2 resulting in a fine black Si−Al−C−N powder. The polymer to ceramic yield was approximately 60−70%.

Anode Preparation. The Si−Al−C−N/CNT composite material was gently crushed using mortar-pestle to obtain a fine powder (approximately 1−2 μm in size, as determined by the SEM). It was then dispersed in a toluene/NMP mixture (1:1 by weight) (ACS reagent) and sonicated for 1 h to obtain uniform dispersions. After keeping the dispersion stable for 12 h, the solution at the top was decanted (concentration observed to be ∼8 mg.mL^{-1}) and later carefully sprayed on heated copper foil by use of an airbrush at 15 psi air pressure. The spraying was done with passes (with a single pass lasting for approximately 5 s followed by 10 s of break) while the substrate surface temperature was raised to approximately 180 °C. Frequent stops between the passes allowed the solvent to evaporate and thereby form a uniform compact coating. Spray coating was carried out until the appropriate dark black coating thickness was visually realized. The coated copper foils were then maintained at 150 °C on a hot plate for approximately 12 h to ensure removal of volatile components. The material loading was measured to be approximately 0.2 mg cm^{-2}. "Neat" Si−C−N, Si−Al−C−N particles, and MWCNT electrodes were also prepared in a similar manner without conducting agent or binders. However, Si−C−N, Si−Al−C−N dispersions were not stable and the coating adhesion to the copper foil was generally poor.

Coin−Cell Assembly. Half-cell batteries were made by punching 14.3 mm diameter out of the foil for use as working electrode. A few drops of electrolyte solution of 1 M $LiPF_6$ (Alfa Aesar) dissolved in (1:1 v/v) dimethyl carbonate: ethylene carbonate (ionic conductivity 10.7 mS cm^{-1}) was used. A glass separator, soaked in electrolyte was placed between the working electrode and pure lithium metal (14.3 mm diameter), which acted as counter electrode. Washer, spring and a top casing were placed on top to complete the assembly before crimping. The whole procedure was carried out in an Ar-filled glovebox.

Electrochemical performance of the assembled coin cells was tested using a multichannel BT2000 Arbin test unit sweeping between 2.5 V to 10 mV vs Li/Li^+ using following cycle schedule: (a) Asymmetric mode: Li was inserted at 0.1 A g^{-1} (w.r.t. weight of the coating), while the extraction was performed at increasing current densities of 0.1, 0.2, 0.4, 0.8, 1.6, 3.2, 6.4, and 10 A g^{-1} for 5 cycles each, and returning back to 0.1 A g^{-1} for the next 10 cycles. (b) Symmetric mode: Later, all the cells were subjected to symmetric cycling at a current density of 1.6 A g^{-1} for up to 1000 cycles, returning back to 0.1 A g^{-1} for the last 100 cycles.

RESULTS AND DISCUSSIONS

Synthesis and Characterization. Supporting Information Figure S1 illustrates the proposed reaction mechanism for Al-doping of poly(ureamethylvinyl)silazane. The addition of aluminum propoxide to polysilazane results in formation of covalent bond between nitrogen and aluminum. Because of steric hindrance it is assumed that aluminum propoxide can undergo reaction with polysilazane at few N−H bonds forming aluminum containing chainlike structures. The schematic in Figure 1 describes the overall approach toward synthesis of Si−Al−C−N/CNT ceramic composite and its subsequent spray coating method for electrode preparation. It is well established that CNTs sidewalls are chemically reactive due to the π orbital misalignment between carbon atoms in CNT.[54] Thus, a strong van der Waals interaction between the aromatic groups in toluene and the $\pi-\pi$ stacking of the CNTs sidewalls exists. A noncovalent interaction between the amine domains from the hydrophobic polymer backbone (locked in place by toluene) and CNTs sidewalls is now possible. This process results in functionalization of CNTs surface with as-synthesized liquid Al-modified polysilazane. During cross-linking step at 300 °C, the propoxy ion from aluminum propoxide combines with weakly bonded hydrogen in Si−N polymer backbone, there-by releasing propanol as a byproduct. This thermal cross-linking leads to a 3D network where aluminum is preferentially enriched in string like regions separated by aluminum-poor regions. On further pyrolysis at 1000 °C, reaction of aluminum alkoxide with Si−H and N−H bonds facilitates distribution of aluminum in flexible chainlike blocks along with large Si−N rings throughout the matrix.[46,56−58]

A range of spectroscopic analyses was performed to confirm the presence of Al in the polymer, its cross-linking behavior, and the functionalization of CNTs with Si−Al−C-N ceramic as proposed in Figure 1. We compared the FTIR spectra of Si−Al−C-N/CNT with its cross-linked polymer counterparts and "neat" CNTs (Figure 2a). The small peak at 3680 cm^{-1} and a broad peak between 3480 and 3400 cm^{-1} are characterized to free and bonded −OH stretching, most likely due to moisture absorption. The FTIR spectrum of polysilazane is similar to what has been previously reported in the literature.[61,62] The peaks ascribed to vinyl groups are the C−H vibrations at 2950 cm^{-1}. The peak attributed to Si-NH-Si group is Si−N vibration at 1160 cm^{-1}. Si-CH_3 characteristic peak was observed at 1253 cm^{-1} and methyl vibrations at 2954 and 2910 cm^{-1}. The large peak at 2111 cm^{-1} is attributed to Si−H. The broad band between 640 and 1000 cm^{-1} is resultant to merger of two bonds: Si−C and Si−N. The major noticeable difference in the Si−Al−C-N/CNT spectra is the peak at 1620 cm^{-1} which corresponds to C═C bond. Further, the Si-CH_3 groups (1253, 2954, and 2896 cm^{-1}) and Si−H peak at 2114 cm^{-1} could not be prominently observed due to elimination of H_2 and methyl groups during pyrolysis. The peaks that cover Si−C, Si−N, Al−N, and C−C at the lower wavenumber range (<1400 cm^{-1}) suggest mixture of bonds.[62−66] Further characterization of the composite was carried out by use of solid-state NMR (^{27}Al). Figure 2b compares the ^{27}Al NMR spectra of Si−Al−C-N/CNT before and after pyrolysis. The spectra obtained before pyrolysis shows one distinct peak at 51 ppm, corresponding to AlN_5 structures. While after pyrolysis a new peak centered at 8 ppm corresponding to AlN_6 evolved along with AlN_5. These results suggest the presence of both pentavalent and hexavalent Al but no 4-fold coordinated aluminum nuclie (generally observed at 100 ppm) could be characterized in the ceramic structure.[39,66,67] On the basis of the FTIR and NMR, analysis we can confirm the broad structure of the amorphous ceramic shell deduced in Figure 1. Additional analysis involved XPS of the Si−Al−C−N/CNT composite material as presented in Figure 2c and d, the survey scans of the specimen showed existence of Si, Al, and C elemental peaks arising from the valence energy levels for the respective atoms. The atomic percentage of Al in Si−Al−C−N and Si−Al−C−N/CNT composites were observed to be 1.11 and 0.79 at. %, respectively. A bar chart in Supporting Information Figure S2 shows the relative percentage of all the elements in Si−Al−C-N and Si−Al−C-N/CNT composites obtained using XPS. The surface atomic composition was observed to be $SiAl_{0.07}C_{2.57}N_{0.35}O_{1.7}$. The peak at about 74.4 eV in the high-resolution Al 2p spectrum as shown in Figure 2d confirmed the presence of Al−N and some Al−O bonds in the composite material. This unambiguously attests the successful introduction of Al into the final ceramic material. The binding energy of the C 1s photoelectrons at ∼284.5 eV suggest $-sp^2$ carbon peak. Further, X-ray diffraction (XRD) spectrum of Si−Al−C−N in Figure 2e substantiated that the material was indeed amorphous which is a typical of PDCs glass-ceramics. The Raman spectrum of the prepared Si−Al−C-N/CNT composite, Figure 2f, displayed characteristic D (∼1350 cm^{-1}) and G (∼1600 cm^{-1}) band, further corroborating the presence of CNTs in the pyrolyzed composite.

Further analysis of the hybrid composite involved thermogravimetric analysis (TGA), presented in Figure 2g, highlighted the extreme thermal stability of Si−Al−C−N ceramic at 1000 °C flowing air, with negligible weight change. While the TGA spectrum of Si−Al−C−N/CNT had a linear relationship between residual mass and oxidation temperature, which was observed to be 680 °C. After the weight loss at about 680 °C, the composite specimen showed stability in their weight. The TGA residual weight was 79% for Si−Al−C−N/CNT specimen. The TGA data for "neat" CNTs on the other hand indicate 98% weight loss at ∼680 °C. Thus, it can be concluded that the composite structure prepared by functionalization of nanotubes with Si−Al−C−N ceramic improved oxidation resistance of CNTs by approximately 80 °C. The weight loss at 680 °C is attributed to the combustion of CNTs in the composite, which suggests that the composite had approximately 30% CNTs by weight (about 25% more than the initial CNT loading in the Al-polymeric precursor).

Transmission electron microscope (TEM) images in Figure 2h and 2i represent CNTs after functionalization by Si−Al−C−N ceramic. HRTEM image in Figure 2i confirmed the formation of composite *nanowire-like* structure consisting of Si−Al−C−N shell on CNT core (additional images in Supporting Information Figure S3). This is further proved by EDX analysis of the image which showed peaks at 0.27, 0.37, 0.52, 1.49, and 1.75 keV, which corresponds to C, N, O, Al and Si, respectively. The TEM diffraction pattern for the composite

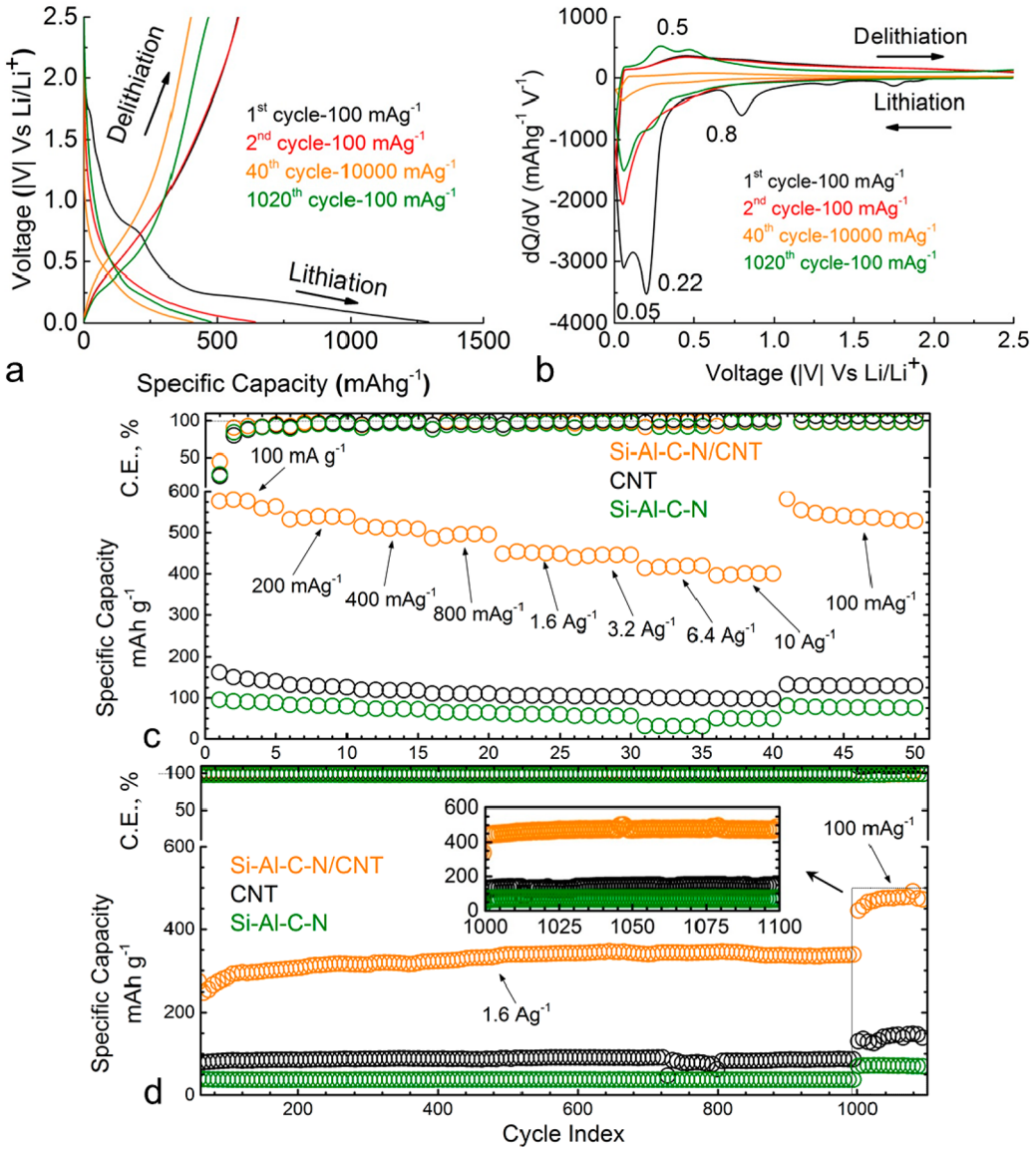

Figure 3. Electrochemical data. 1st, 2nd, 40th, and 1020th cycle (a) voltage profile and (b) differential capacity curve for Si−Al−C−N/CNT hybrid composite electrode. Charge capacity comparison of all electrodes: (c) asymmetrically cycled at different rates for every 5 cycles and (d) consecutively cycled symmetrically at 1600 mA g^{-1} for 1000 cycles. Columbic efficiency is plotted for all the material on the upper portion of the respective graph. The detailed view in the inset shows the extreme stability of Si−Al−C−N/CNT after 1000 cycles. All capacities are based on the total mass of the coated material.

Table 1. Summary of the Experimental Results Compared with Various Precursor-Derived Si−C−N Glass-Ceramic and Composite Electrodes for LIB

material	1st cycle charge (mAh g^{-1})	binder and conductive agents	capacity at max. current density tested (mAh g^{-1})	max. number of cycles tested
Si−Al−C−N/CNT (present work)	577	no	400 (10000 mA g^{-1})	1100
MWCNT (present work)	162	no	98 (10000)	1100
Si−Al−C−N (present work)	96	no	50 (10000)	1100
graphite[69]	298	yes	240 (50)	50
SiCN-1100 °C[31]	263	yes	100 (36)	50
SiCN-1300 °C/O_2[31]	291	yes	250 (72)	60
SiCN-1100 °C[32]	254	yes	95 (360)	10
SiCN-1000 °C[33]	456	yes	171 (100)	30
SiCN-graphite[49]	312	yes	200 (720)	275
SiCN-graphene[50]	420	yes	440 (40)	50
Si(B)CN-CNT[51]	362	yes	430 (100)	30

was featureless thus confirming the amorphous nature of Si−Al−C−N. Figure 2j shows the SEM image of the spray-coated specimen, which suggests that the uniform particle sized composite material, has evenly covered the copper foil. The EDX spectra in the inset from the marked spot in the corresponding SEM image showed peaks at 0.27, 0.37, 0.52, 1.49, and 1.75 keV, which corresponds to C, N, O, Al and Si, respectively.

Electrochemical Cycling Results. Electrochemical behavior of the synthesized hybrid ceramic was studied by cycling it in a half-cell configuration against pure lithium metal. The loading of the active material was measured to be approximately 0.2 mg cm^{-2}. Figure 3a and 3b shows the charge/discharge profile and differential capacity curves of first two cycles for the hybrid composite electrode. First cycle discharge and charge capacity were observed to be 1294 and 577 mAh g^{-1}. This suggests that large percentage of Li is still consumed during SEI formation; however, this initial loss of Li maybe lowered by prelithiation in future studies. The capacity is among the highest reported for any polymer derived ceramics (Table 1). Further, the differential capacity curve showed reduction peaks typical to PDCs at 50, 220, and 800 mV and oxidation peak at 500 mV. The charge/discharge profile and differential capacity curves of spray coated "neat" CNTs, Si−Al−C−N, and SiCN ceramic (without binder or conducting agents) are compared in the Supporting Information Figure S4. Even though the first cycle discharge capacity of CNTs was relatively high at ∼670 mAh g^{-1}, it suffered from a large first cycle loss showing charge capacity of ∼200 mAh g^{-1}. In case of the ceramic particle anodes the electrochemical performance was extremely low relative to the hybrid composite anode. The spray coated Si−C−N electrode performed poorly (first cycle charge capacity of 50 $mAhg^{-1}$ at 100 mAg^{-1}) and its cycling was stopped after first two cycles. Both the neat CNTs and Si−Al−C−N ceramic electrodes' differential capacity curves had a major reduction peak at 0.05 V which is attributed to Li ion intercalation and another peak at 0.8 V which is attributed to SEI formation as this peak disappeared during the second cycle. In case of Si−Al−C−N there were additional peaks centered at 1.44, 1.74, and 2.07 V.

On further cycling (Figure 3c), Si−Al−C−N/CNT maintained its high capacity at ∼564 mAh g^{-1} (with 98% of the initial capacity retained) which is relatively high when compared to "neat" CNTs and Si−Al−C−N with charge capacities of ∼140 and ∼88 mAh g^{-1}, respectively after 5 cycles at 0.1 A g^{-1}. Later, the current density was gradually increased to 0.2, 0.4, 0.8, 1.6, 3.2, 6.4, and 10 A g^{-1} for each 5 cycles consecutively. Impressively, Si−Al−C−N/CNT hybrid composite showed reversible capacity of 400 mAh g^{-1} even at 10 A g^{-1} which was approximately 70% of the first cycle charge capacity. When the cells were cycled back at 0.1 A g^{-1}, all the cells regained their initial charge capacities at 540, 130, and 77 mAh g^{-1} for Si−Al−C−N/CNT, CNTs and Si−Al−C−N, respectively. Similar trend was observed in areal charge capacity data, which is presented in Supporting Information Figure S5.

Long-term cycling behavior was studied by cycling symmetrically at 1.6 A g^{-1} for approximately 1000 cycles (Figure 3d). Si−Al−C−N/CNT had an impressively stable and high charge capacity of ∼342 mAh·g^{-1} (60% capacity retention) than CNTs and Si−Al−C−N anode at ∼91 and 37 mAh g^{-1}, respectively. A slight rise in capacity for the initial cycles at high current density could be due to creation for defects in the partially or uncoated nanotubes[60] that allowed additional Li storage sites. Nonetheless, all the cells regained most of their initial capacity when they were cycled back to the lower current density of 0.1 A g^{-1} after 1000 cycles. Si−Al−C−N/CNT was the best performing anode with 468 mAh g^{-1} (81% retention w.r.t. first cycle) at 0.1 A g^{-1} after 1000 cycles at 1.6 A g^{-1} during both discharge and charge half cycles. The Si−Al−C−N/CNT electrode represents considerable improvement over other polysilazane derived siliconcarbonitride ceramic and composite electrodes (with carbon nanotube and graphene prepared through slurry coating) reported in the literature.[61−65]

The improvement in electrochemical performance of Si−Al−C−N/CNT electrode can be attributed to following synergistic effects: (1) 3-dimensional nature of the PDC electrode due to interfacing with CNTs and increase in surface area, making the electrode more ion-accessible while still maintaining an integral electrical and mechanical contact with the ceramic shell throughout the electrode and the copper current collector foil, respectively, and (2) the robust nanodomain structure and improved electrical conductivity due to Al doping of Si−C−N that improved ceramic's Li-cyclability and simultaneously provided protection to high current carrying CNTs against exfoliation at extreme C-rates. The electrical conductivity of Si−Al−C−N ceramic (measured using four-point technique) was $\sim 1.39 \times 10^{-3}$ S cm^{-1} which is many folds higher than polysilazane-derived Si−C−N with a reported conductivity of approximately 1×10^{-7} S cm^{-1}.[47,58,65] With CNTs embedded in the matrix, the conductivity further increased to approximately 1.55 S cm^{-1} which is close to the measured conductivity of neat MWCNTs of approximately 4.22 S cm^{-1}, there-by making the composite conducting enough to eliminate conductive agents during electrode preparation.

Later, the cells were disassembled in their lithiated state to study the effect of long-term cycling on their morphology and chemical structure. Figure 4 shows the optical photograph, high-resolution SEM and TEM image of Si−Al−C−N/CNT electrode after 1100 cycles along with EDX using HRTEM, respectively. SEM and optical images of all other cycled electrodes are presented in Supporting Information Figure S6. Remarkably, Si−Al−C−N/CNT and CNTs specimens looked intact with no large or micro surface cracks. Further, stable SEI layer formation and the presence of glass fiber separator could be observed (Figure 4a) in the optical image. However, in the case of Si−Al−C−N and Si−C−N particle electrodes, delamination of material from the copper current collector was clearly evident. This was hardly surprising considering the dispersions made with Si−Al−C−N or Si−C−N particles were relatively unstable and the adhesion of the spray-coated particles to the current collector foil was generally poor (Supporting Information Figure S6). On closer examination using SEM, some micro cracks were observed on the surface of the cycled electrode and the charge capacity degradation as observed in the long term cycling data could be attributed to these cracks. TEM image of the cycled Si−Al−C−N/CNT electrodes in Figure 4c,d and Supporting Information Figure S7 indicated SEI formation on the surface of nanotubes. Remarkably, HRTEM images in Figure 4d showed that when compared to the composite material before cycling, the overall composite nanostructure still looked largely intact with complete CNT core structure and unbroken Si−Al−C−N coating being retained. EDX analysis of the HRTEM image in Figure 4e showed presence of Si and Al which further articulates the presence of intact coating on the surface of CNTs. Phosphorus and fluorine at 0.68 and 2.02 keV were also

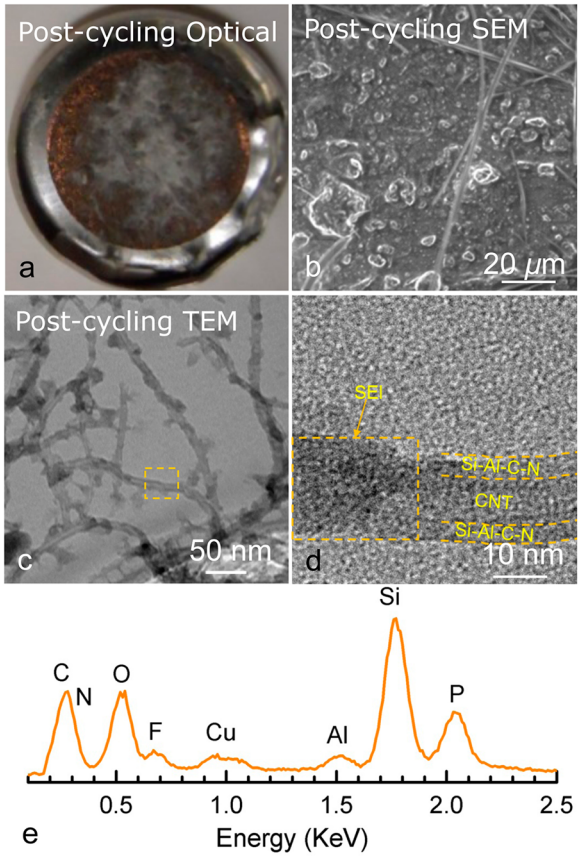

Figure 4. Postcycling microscopy. (a) Optical, (b) SEM, (c) low, and (d) high resolution TEM images of dissembled Si−Al−C−N/CNT electrode after 1100 cycles. Optical image shows glass separator residue as white cotton like material on the surface of electrode. TEM shows CNTs to be still long and intact while the HRTEM shows that the core−shell structure is largely intact. (e) EDX of HRTEM highlights the presence of Si and Al elements in the shell along with high levels of F and P originating from the electrolyte/SEI layer formation. The cell was dissembled in lithiated state.

detected originating from the SEI layer formation on individual nanotubes.

CONCLUSION

Synthesis of Si−Al−C−N/CNT shell/core composite by controlled thermal conversion of Al-modified polysilazane single-source precursor on the surfaces of carbon nanotubes is demonstrated. Electron microscopy and multiple spectroscopic techniques revealed the morphology and chemical structure of the pyrolyzed glass-ceramic shell. TGA analysis highlighted the incredible thermal stability of the composite in flowing air up to 700 °C. Further, we showed that stable dispersions in NMP/Toluene at a concentration of approximately 8 mg.mL^{-1} could be spray-coated on Cu current collector foil as a fast method of binder-free electrode preparation for Li-ion battery anode. Si−Al−C-N/CNTs electrode had an impressive charge capacity of 400 mAh g^{-1} even at 10,000 mA g^{-1} which was 70% of its initial reversible capacity. Long-term symmetrical cycling for 1000 cycles at 1600 mA g^{-1} showed an equally impressive stable charge capacity of ∼350 mAh g^{-1} with near 100% efficiency. Lastly, postcycling electron microscopy of the electrode showed that the coating was largely intact, highlighting the robust nature of precursor-derived ceramics toward repeated Li-ion cycling.

ASSOCIATED CONTENT

Supporting Information

Reaction schematic, TEM images of as-synthesize Si−Al−C−N/CNT material, discharge/charge voltage profiles corresponding to CNTs, Si−Al−C−N, and Si−C−N spray coated electrodes, areal-capacity plots, and Post cycling electrode images. This material is available free of charge via the Internet at http://pubs.acs.org.

AUTHOR INFORMATION

Corresponding Author

*E-mail: gurpreet@ksu.EDU. Tel.: +1-785-532-7085. Fax: +1-785-532-7057.

Notes

The authors declare the following competing financial interest(s): Patent filed: Provisional Patent Application No. 62/022,000; Titled: Synthesis and Extreme Rate Capability of Si−Al−C−N Functionalized Carbon Nanotube Spray-On Coatings As Li-Ion Battery Electrode; Filed: July 8, 2014; Dkt. 46574-PRO.

ACKNOWLEDGMENTS

G.S. thanks Gary Zito (Colorado School of Mines) for assistance with transmission electron microscopy and Dr. Elisabeth Mansfield (NIST) for the chemical vapor deposition furnace. Some portion of this research is based on work supported by the National Science Foundation-Chemical, Bioengineering, Environmental, and Transport Systems Division (CBET) under grant no. 1335862 to G.S. under program manager Dr. Sumanta Acharya. NSF award CHE-0840515 for instrumentation used at the University of Kansas Solid State NMR Facility.

REFERENCES

(1) Armand, M.; Tarascon, J. M. Building Better Batteries. *Nature* **2008**, *451*, 652−657.
(2) Tarascon, J. M.; Armand, M. Issues and Challenges Facing Rechargeable Lithium Batteries. *Nature* **2001**, *414*, 359−367.
(3) Goodenough, J. B.; Kim, Y. Challenges for Rechargeable Li Batteries. *Chem. Mater.* **2010**, *22*, 587−603.
(4) Arico, A. S.; Bruce, P.; Scrosati, B.; Tarascon, J. M.; Van Schalkwijk, W. Nanostructured Materials for Advanced Energy Conversion and Storage Devices. *Nat. Mater.* **2005**, *4*, 366−377.
(5) Choi, N. S.; Chen, Z.; Freunberger, S. A.; Ji, X.; Sun, Y. K.; Amine, K.; Yushin, G.; Nazar, L. F.; Cho, J.; Bruce, P. G. Challenges Facing Lithium Batteries and Electrical Double-Layer Capacitors. *Angew. Chem., Int. Ed.* **2012**, *51*, 9994−10024.
(6) Kamat, P. V. Electrochemistry in the Driver's Seat. *J. Phys. Chem. Lett.* **2011**, *2*, 242−251.
(7) Manthiram, A. Materials Challenges and Opportunities of Lithium Ion Batteries. *J. Phys. Chem. Lett.* **2011**, *2*, 176−184.
(8) Aurbach, D. Review of Selected Electrode-Solution Interactions Which Determine the Performance of Li and Li Ion Batteries. *J. Power Sources* **2000**, *89*, 206−218.
(9) Besenhard, J. O.; Yang, J.; Winter, M. Will Advanced Lithium-Alloy Anodes Have a Chance in Lithium-Ion Batteries? *J. Power Sources* **1997**, *68*, 87−90.
(10) Park, C. M.; Kim, J. H.; Kim, H.; Sohn, H. J. Li-Alloy Based Anode Materials for Li Secondary Batteries. *Chem. Soc. Rev.* **2010**, *39*, 3115−3141.
(11) McDowell, M. T.; Lee, S. W.; Nix, W. D.; Cui, Y. 25th Anniversary Article: Understanding the Lithiation of Silicon and Other Alloying Anodes for Lithium-Ion Batteries. *Adv. Mater.* **2013**, *25*, 4966−4984.

(12) Nadimpalli, S. P. V.; Sethuraman, V. A.; Dalavi, S.; Lucht, B.; Chon, M. J.; Shenoy, V. B.; Guduru, P. R. Quantifying Capacity Loss Due to Solid-Electrolyte-Interphase Layer Formation on Silicon Negative Electrodes in Lithium-Ion Batteries. *J. Power Sources* **2012**, *215*, 145−151.
(13) Beaulieu, L. Y.; Eberman, K. W.; Turner, R. L.; Krause, L. J.; Dahn, J. R. Colossal Reversible Volume Changes in Lithium Alloys. *Electrochem. Solid-State Lett.* **2001**, *4*, A137−A140.
(14) Hatchard, T. D.; Dahn, J. R. In Situ XRD and Electrochemical Study of the Reaction of Lithium with Amorphous Silicon. *J. Electrochem. Soc.* **2004**, *151*, A838−A842.
(15) Wu, H.; Cui, Y. Designing Nanostructured Si Anodes for High Energy Lithium Ion Batteries. *Nano Today* **2012**, *7*, 414−429.
(16) Park, M. H.; Kim, M. G.; Joo, J.; Kim, K.; Kim, J.; Ahn, S.; Cui, Y.; Cho, J. Silicon Nanotube Battery Anodes. *Nano Lett.* **2009**, *9*, 3844−3847.
(17) Song, T.; Xia, J.; Lee, J. H.; Lee, D. H.; Kwon, M. S.; Choi, J. M.; Wu, J.; Doo, S. K.; Chang, H.; Il Park, W.; Zang, D. S.; Kim, H.; Huang, Y.; Hwang, K. C.; Rogers, J. A.; Paik, U. Arrays of Sealed Silicon Nanotubes as Anodes for Lithium Ion Batteries. *Nano Lett.* **2010**, *10*, 1710−1716.
(18) Hu, L.; Xu, K. Nonflammable Electrolyte Enhances Battery Safety. *Proc. Natl. Acad. Sci. U.S.A.* **2014**, *111*, 3205−3206.
(19) Lim, S.; Yoon, C. S.; Cho, J. Synthesis of Nanowire and Hollow $LiFePO_4$ Cathodes for High-Performance Lithium Batteries. *Chem. Mater.* **2008**, *20*, 4560−4564.
(20) Liu, B.; Soares, P.; Checkles, C.; Zhao, Y.; Yu, G. Three-Dimensional Hierarchical Ternary Nanostructures for High-Performance Li-Ion Battery Anodes. *Nano Lett.* **2013**, *13*, 3414−3419.
(21) Ruvinskiy, P.; Barsukov, I. V.; Mashtalir, O.; Reid, C. M.; Wu, J. J.; Gogotsi, Y. Nano-Silicon Containing Composite Graphitic Anodes with Improved Cycling Stability for Application in High Energy Lithium-Ion Batteries. *ECS J. Solid State Sci. Technol.* **2013**, *2*, M3028−M3033.
(22) Kim, H.; Seo, M.; Park, M. H.; Cho, J. A Critical Size of Silicon Nano-Anodes for Lithium Rechargeable Batteries. *Angew. Chem., Int. Ed.* **2010**, *49*, 2146−2149.
(23) Chockla, A. M.; Klavetter, K. C.; Mullins, C. B.; Korgel, B. A. Tin-Seeded Silicon Nanowires for High Capacity Li-Ion Batteries. *Chem. Mater.* **2012**, *24*, 3738−3745.
(24) Chan, C. K.; Patel, R. N.; O'Connell, M. J.; Korgel, B. A.; Cui, Y. Solution-Grown Silicon Nanowires for Lithium-Ion Battery Anodes. *ACS Nano* **2010**, *4*, 1443−1450.
(25) Luo, J.; Zhao, X.; Wu, J.; Jang, H. D.; Kung, H. H.; Huang, J. Crumpled Graphene-Encapsulated Si Nanoparticles for Lithium Ion Battery Anodes. *J. Phys. Chem. Lett.* **2012**, *3*, 1824−1829.
(26) Mera, G.; Tamayo, A.; Nguyen, H.; Sen, S.; Riedel, R. Nanodomain Structure of Carbon-Rich Silicon Carbonitride Polymer-Derived Ceramics. *J. Am. Ceram. Soc.* **2010**, *93*, 1169−1175.
(27) Morcos, R. M.; Mera, G.; Navrotsky, A.; Varga, T.; Riedel, R.; Poli, F.; Mueller, K. Enthalpy of Formation of Carbon-Rich Polymer-Derived Amorphous SiCN Ceramics. *J. Am. Ceram. Soc.* **2008**, *91*, 3349−3354.
(28) Kaspar, J.; Terzioglu, C.; Ionescu, E.; Graczyk-Zajac, M.; Hapis, S.; Kleebe, H. J.; Riedel, R. Stable SiOC/Sn Nanocomposite Anodes for Lithium-Ion Batteries with Outstanding Cycling Stability. *Adv. Funct. Mater.* **2014**, *24*, 4097−4104.
(29) Fukui, H.; Nakata, N.; Dokko, K.; Takemura, B.; Ohsuka, H.; Hino, T.; Kanamura, K. Lithiation and Delithiation of Silicon Oxycarbide Single Particles with a Unique Microstructure. *ACS Appl. Mater. Interfaces* **2011**, *3*, 2318−2322.
(30) Ahn, D.; Raj, R. Cyclic Stability and C-Rate Performance of Amorphous Silicon and Carbon Based Anodes for Electrochemical Storage of Lithium. *J. Power Sources* **2011**, *196*, 2179−2186.
(31) Shen, J.; Raj, R. Silicon-Oxycarbide Based Thin Film Anodes for Lithium Ion Batteries. *J. Power Sources* **2011**, *196*, 5945−5950.
(32) Fukui, H.; Ohsuka, H.; Hino, T.; Kanamura, K. Polysilane/Acenaphthylene Blends Toward Si−O−C Composite Anodes for Rechargeable Lithium-Ion Batteries. *J. Electrochem. Soc.* **2011**, *158*, A550−A555.
(33) Graczyk-Zajac, M.; Mera, G.; Kaspar, J.; Riedel, R. Electrochemical Studies of Carbon-Rich Polymer-Derived SiCN Ceramics as Anode Materials for Lithium-Ion Batteries. *J. Eur. Ceram. Soc.* **2010**, *30*, 3235−3243.
(34) Kaspar, J.; Mera, G.; Nowak, A. P.; Graczyk-Zajac, M.; Riedel, R. Electrochemical Study of Lithium Insertion Into Carbon-Rich Polymer-Derived Silicon Carbonitride Ceramics. *Electrochim. Acta* **2010**, *56*, 174−182.
(35) Su, D.; Li, Y. L.; Feng, Y.; Jin, J. Electrochemical Properties of Polymer-Derived SiCN Materials as the Anode in Lithium Ion Batteries. *J. Am. Ceram. Soc.* **2009**, *92*, 2962−2968.
(36) Tamai, H.; Sugahara, H.; Yasuda, H. Preparation of Carbons from Pitch Containing Polysilane and Their Anode Properties for Lithium-Ion Batteries. *J. Mater. Sci. Lett.* **2000**, *19*, 53−56.
(37) Ahn, D.; Raj, R. Thermodynamic Measurements Pertaining to the Hysteretic Intercalation of Lithium in Polymer-Derived Silicon Oxycarbide. *J. Power Sources* **2010**, *195*, 3900−3906.
(38) Sarkar, S.; Gan, Z.; An, L.; Zhai, L. Structural Evolution of Polymer-Derived Amorphous SiBCN Ceramics at High Temperature. *J. Phys. Chem. C* **2011**, *115*, 24993−25000.
(39) Dhamne, A.; Xu, W. X.; Fookes, B. G.; Fan, Y.; Zhang, L. G.; Burton, S.; Hu, J. Z.; Ford, J.; An, L. A. Polymer-Ceramic Conversion of Liquid Polyaluminasilazanes for SiAlCN Ceramics. *J. Am. Ceram. Soc.* **2005**, *88*, 2415−2419.
(40) Hermann, A. M.; Wang, Y. T.; Ramakrishnan, P. A.; Balzar, D.; An, L. N.; Haluschka, C.; Riedel, R. Structure and Electronic Transport Properties of Si−(B)−C−N Ceramics. *J. Am. Ceram. Soc.* **2001**, *84*, 2260−2264.
(41) Bhandavat, R.; Singh, G. Synthesis, Characterization, and High Temperature Stability of Si(B)CN-Coated Carbon Nanotubes Using a Boron-Modified Poly(Ureamethylvinyl)Silazane Chemistry. *J. Am. Ceram. Soc.* **2012**, *95*, 1536−1543.
(42) An, L. N.; Wang, Y. G.; Bharadwaj, L.; Zhang, L. G.; Fan, Y.; Jiang, D. P.; Sohn, Y. H.; Desai, V. H.; Kapat, J.; Chow, L. C. Silicoaluminum Carbonitride With Anomalously High Resistance to Oxidation and Hot Corrosion. *Adv. Eng. Mater.* **2004**, *6*, 337−340.
(43) Riedel, R.; Kienzle, A.; Dressler, W.; Ruwisch, L.; Bill, J.; Aldinger, F. A Silicoboron Carbonitride Ceramic Stable to 2,000 °C. *Nature* **1996**, *382*, 796−798.
(44) An, L. A.; Riedel, R.; Konetschny, C.; Kleebe, H. J.; Raj, R. Newtonian Viscosity of Amorphous Silicon Carbonitride at High Temperature. *J. Am. Ceram. Soc.* **1998**, *81*, 1349−1352.
(45) Riedel, R.; Ruswisch, L. M.; An, L. N.; Raj, R. Amorphous Silicoboron Carbonitride Ceramic With Very High Viscosity at Temperatures Above 1500 °C. *J. Am. Ceram. Soc.* **1998**, *81*, 3341−3344.
(46) Zimmermann, A.; Bauer, A.; Christ, M.; Cai, Y.; Aldinger, F. High-Temperature Deformation of Amorphous Si−C−N and Si−B−C−N Ceramics Derived from Polymers. *Acta Mater.* **2002**, *50*, 1187−1197.
(47) Ramakrishnan, P. A.; Wang, Y. T.; Balzar, D.; An, L. A.; Haluschka, C.; Riedel, R.; Hermann, A. M. Silicoboron-Carbonitride Ceramics: A Class of High-Temperature, Dopable Electronic Materials. *Appl. Phys. Lett.* **2001**, *78*, 3076−3078.
(48) Liebau-Kunzmann, V.; Fasel, C.; Kolb, R.; Riedel, R. Lithium Containing Silazanes as Precursors for SiCN: Li Ceramics—A Potential Material for Electrochemical Applications. *J. Eur. Ceram. Soc.* **2006**, *26*, 3897−3901.
(49) Chen, J.; Liu, Y.; Minett, A. I.; Lynam, C.; Wang, J.; Wallace, G. G. Flexible, Aligned Carbon Nanotube/Conducting Polymer Electrodes for a Lithium-Ion Battery. *Chem. Mater.* **2007**, *19*, 3595−3597.
(50) Feng, Y.; Du, G. X.; Zhao, X. J.; Yang, E. C. Preparation and Electrochemical Performance of SiCN-CNTs Composite Anode Material for Lithium Ion Batteries. *J. Appl. Electrochem.* **2011**, *41*, 999−1002.
(51) Graczyk-Zajac, M.; Fasel, C.; Riedel, R. Polymer-Derived-SiCN Ceramic/Graphite Composite as Anode Material with Enhanced Rate

Capability for Lithium Ion Batteries. *J. Power Sources* **2011**, *196*, 6412−6418.
(52) Kolb, R.; Fasel, C.; Liebau-Kunzmann, V.; Riedel, R. SiCN/C-Ceramic Composite as Anode Material for Lithium Ion Batteries. *J. Eur. Ceram. Soc.* **2006**, *26*, 3903−3908.
(53) Bhandavat, R.; Singh, G. Improved Electrochemical Capacity of Precursor-Derived Si(B)CN-Carbon Nanotube Composite as Li-Ion Battery Anode. *ACS Appl. Mater. Interfaces* **2012**, *4*, 5092−5097.
(54) Hirsch, A. Functionalization of Single-Walled Carbon Nanotubes. *Angew. Chem., Int. Ed.* **2002**, *41*, 1853−1859.
(55) Lee, W. J.; Hwang, T. H.; Hwang, J. O.; Kim, H. W.; Lim, J.; Jeong, H. Y.; Shim, J.; Han, T. H.; Kim, J. Y.; Choi, J. W.; Kim, S. O. N-Doped Graphitic Self-Encapsulation for High Performance Silicon Anodes in Lithium-Ion Batteries. *Energy Environ. Sci.* **2014**, *7*, 621−626.
(56) Lee, W. J.; Lee, D. H.; Han, T. H.; Lee, S. H.; Moon, H.-S.; Lee, J. A.; Kim, S. O. Biomimetic Mineralization of Vertical N-Doped Carbon Nanotubes. *Chem. Commun.* **2011**, *47*, 535−537.
(57) Lee, W. J.; Lee, J. M.; Kochuveedu, S. T.; Han, T. H.; Jeong, H. Y.; Park, M.; Yun, J. M.; Kwon, J.; No, K.; Kim, D. H.; Kim, S. O. Biomineralized N-Doped CNT/TiO_2 Core/Shell Nanowires for Visible Light Photocatalysis. *ACS Nano* **2012**, *6*, 935−943.
(58) Nakashima, H.; Koyama, S.; Kuroda, K.; Sugahara, Y. Conversion Of A Precursor Derived From Cage-Type and Cyclic Molecular Building Blocks into Al−Si−N−C Ceramic Composites. *J. Am. Ceram. Soc.* **2002**, *85*, 59−64.
(59) Pinkas, J.; Wang, T. L.; Jacobson, R. A.; Verkade, J. G. Azaaluminatranes Exhibiting Unusual Coordination Geometries for Aluminum. *Inorg. Chem.* **1994**, *33*, 4202−4210.
(60) Shin, W. H.; Jeong, H. M.; Kim, B. G.; Kang, J. K.; Choi, J. W. Nitrogen-Doped Multiwall Carbon Nanotubes for Lithium Storage with Extremely High Capacity. *Nano Lett.* **2012**, *12*, 2283−2288.
(61) Akitt, J. W. Multinuclear Studies of Aluminum Compounds. *Prog. Nucl. Magn. Reson. Spectrosc.* **1989**, *21*, 1.
(62) Li, Y. L.; Kroke, E.; Riedel, R.; Fasel, C.; Gervais, C.; Babonneau, F. Thermal Cross-Linking and Pyrolytic Conversion of Poly(Ureamethylvinyl)silazanes to Silicon-Based Ceramics. *Appl. Organomet. Chem.* **2001**, *15*, 820−832.
(63) Antsiferov, V. N.; Gilyov, V. G.; Karmanov, V. I. IR-Spectra and Phases Structure of SiAlONs. *Vib. Spectrosc.* **2002**, *30*, 169−173.
(64) Wada, N.; Solin, S. A.; Wong, J.; Prochazka, S. Raman and IR Absorption Spectroscopic Studies on Alpha, Beta, and Amorphous Si_3N_4. *J. Non-Cryst. Solids* **1981**, *43*, 7−15.
(65) Ermer, E.; Ptak, W. S. FTIR Studies of Structural Effects Due to Boron Addition in Sintered Silicon Carbide. *Vib. Spectrosc.* **2002**, *29*, 211−215.
(66) Lv, Q.; Cao, C. B.; Li, C.; Zhang, J. T.; Zhu, H. X.; Kong, X.; Duan, X. F. Formation of Crystalline Carbon Nitride Powder by a Mild Solvothermal Method. *J. Mater. Chem.* **2003**, *13*, 1241−1243.
(67) Berger, F.; Weinmann, M.; Aldinger, F.; Muller, K. Solid-State NMR Studies of the Preparation of Si−Al−C−N Ceramics from Aluminum-Modified Polysilazanes and Polysilylcarbodiimides. *Chem. Mater.* **2004**, *16*, 919−929.
(68) Verdecia, G.; O'Brien, K. L.; Schmidt, W. R.; Apple, T. M. Aluminum-27 and Silicon-29 Solid-State Nuclear Magnetic Resonance Study of Silicon Carbide Aluminum Nitride Systems: Effect of Silicon/Aluminum Ratio and Pyrolysis Temperature. *Chem. Mater.* **1998**, *10*, 1003−1009.
(69) Wang, C.; Li, D.; Too, C. O.; Wallace, G. G. Electrochemical Properties of Graphene Paper Electrodes Used in Lithium Batteries. *Chem. Mater.* **2009**, *21*, 2604−2606.